HHS Public Access

Author manuscript

Environ Sci Technol. Author manuscript; available in PMC 2017 July 10.

Published in final edited form as:

Environ Sci Technol. 2016 April 19; 50(8): 4248–4258. doi:10.1021/acs.est.5b04834.

Real-Time Manganese Phase Dynamics during Biological and Abiotic Manganese Oxide Reduction

Jena E. Johnson[*,†,#], **Pratixa Savalia**[‡], **Ryan Davis**[§], **Benjamin D. Kocar**[‖], **Samuel M. Webb**[§], **Kenneth H. Nealson**[‡], and **Woodward W. Fischer**[†]

[†]Division of Geological and Planetary Sciences, California Institute of Technology, Pasadena, California 91125, United States

[‡]University of Southern California, Los Angeles, California 90089, United States

[§]Stanford Synchrotron Radiation Lightsource, Menlo Park, California 94025, United States

[‖]Massachusetts Institute of Technology, Cambridge, Massachusetts 02139, United States

Abstract

Manganese oxides are often highly reactive and easily reduced, both abiotically, by a variety of inorganic chemical species, and biologically during anaerobic respiration by microbes. To evaluate the reaction mechanisms of these different reduction routes and their potential lasting products, we measured the sequence progression of microbial manganese(IV) oxide reduction mediated by chemical species (sulfide and ferrous iron) and the common metal-reducing microbe *Shewanella oneidensis* MR-1 under several endmember conditions, using synchrotron X-ray spectroscopic measurements complemented by X-ray diffraction and Raman spectroscopy on precipitates collected throughout the reaction. Crystalline or potentially long-lived phases produced in these experiments included manganese(II)-phosphate, manganese(II)-carbonate, and manganese(III)-oxyhydroxides. Major controls on the formation of these discrete phases were alkalinity production and solution conditions such as inorganic carbon and phosphate availability. The formation of a long-lived Mn(III) oxide appears to depend on aqueous Mn^{2+} production and the relative proportion of electron donors and electron acceptors in the system. These real-time measurements identify mineralogical products during Mn(IV) oxide reduction, contribute to understanding the mechanism of various Mn(IV) oxide reduction pathways, and assist in interpreting the processes occurring actively in manganese-rich environments and recorded in the geologic record of manganese-rich strata.

Graphical abstract

[*]Corresponding Author: jena@gps.caltech.edu.

[#]**Present Address**

Department of Geological Sciences, University of Colorado, Boulder, CO 80309; jena.johnson@colorado.edu; 303-492-7025.

Notes

The authors declare no competing financial interest.

Supporting Information

The Supporting Information is available free of charge on the ACS Publications website at DOI: 10.1021/acs.est.5b04834.

Additional figures and tables that show supplemental results and support conclusions reported in this manuscript (PDF)

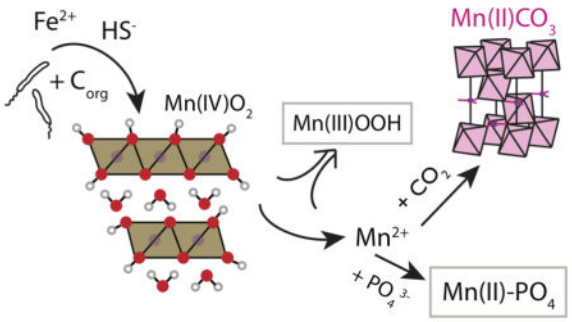

INTRODUCTION

The cycling of manganese is critically important for the sequestration of toxins and trace metals, the neutralization of reactive oxygen species, and interactions with carbon, sulfur, and iron.[1] Amorphous and poorly crystalline manganese(III,IV) oxides are highly favorable electron acceptors for microbial anaerobic respiration,[2–4] an important process in both marine sediments and terrestrial environments.[5–7] But manganese oxides can also be reduced chemically by many inorganic species, including Fe^{2+}, sulfide, arsenite, and uraninite.[8–11] Thus, Mn(III,IV) oxides are often rapidly cycled in sediments and soils as they undergo many reduction and reoxidation reactions.[1,6,12,13]

After reduction of manganese(III,IV) oxides, the resultant Mn(II) can either be reoxidized, incorporated into a Mn(II)-precipitate and immobilized in soils and sediments, or aqueous and soluble Mn^{2+} can be released to pore fluids and groundwater.[5,13,14] Dynamic manganese cycling occurs across a range of subsurface environments, including the oxic–anoxic boundaries in soils and marine sediments, suboxic water columns, and acid mine drainage areas.[15–18] Currently, it is unclear which reductants and what environmental conditions control the behavior of reduced manganese and its potential to become “fixed” in minerals or released for future reactions. The high redox potentials of manganese oxides result in multiple possible Mn(IV) reduction pathways via a variety of competing reductants,[14] wherein Mn(IV) could pass through Mn(III) intermediates[19,20] or be directly reduced to Mn(II).[21] Additionally, the changes in dissolved inorganic carbon and pH during different Mn(IV) reduction reactions might promote the precipitation of Mn(II)-carbonate[5,22] or other Mn(II) minerals that remove manganese from the solution, or alternatively produce aqueous Mn^{2+} that could be advected away for further cycling.[5,14]

The potential for the sequestration of manganese in minerals is also relevant for the interpretation of the geologic record of manganese-rich sedimentary rocks. The rock record of manganese is dominated by Mn-bearing carbonates (rhodochrosite, $MnCO_3$, or kutnohorite, $MnCa(CO_3)_2$) and a Mn(III) phase (braunite, $Mn(III)_6Mn(II)SiO_{12}$).[23–26] The occurrence of Mn(II+III) minerals in ancient sediments is notable because manganese is deposited primarily as Mn(IV) oxides.[1,27–32] These phases confirm modern observations[5,6,12–14,33] that reductive processes occur frequently in sediments after Mn(IV) oxide deposition, but the diagenetically stable mineral products associated with the various reduction reactions are not well-known. Many previous workers have hypothesized that

ancient Mn-carbonates were once Mn(IV) oxides that were secondarily reduced by organic carbon, potentially in microbially mediated reactions.[25,26,34–37] Rhodochrosite has been observed as a product of microbial respiration of Mn oxides previously[2,10,22] although it was not studied extensively for the requisite conditions of precipitation. Other studies have measured Mn-carbonate production during microbial sulfate reduction or thiosulfate disproportionation from secondary abiotic interactions between sulfide and Mn-oxides.[38–41]

To our knowledge, only one study has measured a real-time reaction sequence of Mn(IV) oxide reduction, using time-resolved X-ray diffraction (XRD) measurements.[42] Fischer et al. reacted powdered birnessite (a layered Mn(III,IV) oxide) with total membrane extracts from a common and well-studied metal-reducing microbe, *Shewanella oneidensis* MR-1. They observed the mineralogical changes that occurred, finding production of rhodochrosite and hausmannite (Mn_3O_4). This XRD-based in vitro study helped identify mineralogical products derived from the reduction of birnessite; here we follow up on this work to examine the mineralogical changes and products that occur during Mn(IV) reduction by live microbes in a more realistic experimental system.

To better understand the environmental and mechanistic controls on mineral products from Mn oxide reduction with various reductants, we developed a flexible in vivo system to gather time-resolved measurements of the redox and phase changes that occur during various inorganic and organic microbially mediated Mn reduction pathways. Observing the reduction sequence progressions for a given experiment both constrains the reduction mechanism and reveals reaction transient phases during Mn reduction reactions. These transient phases may be stabilized as long-lived products if Mn reduction is reductant-limited, introducing another set of possible outcomes. We also specifically probed the biological reduction mechanism of the manganese-reducing microbe *S. oneidensis* MR-1 (one of the many manganese-reducing *Shewanella* strains[43]) using experiments supplemented with a strong Mn^{2+} ligand—phosphate—to see when and how Mn^{2+} was formed during manganese oxide respiration as compared to phosphate-free reduction sequences. Reduction progressions from abiotic manganese oxide reduction using ferrous iron and sulfide were also observed as inorganic examples. By unraveling the mechanisms controlling the formation of various intermediates and products during common Mn(IV) oxide reduction pathways, we can begin to link the formation of certain key Mn minerals to the interplay between solution conditions and reduction processes.

MATERIALS AND METHODS

Abiotic and biologically mediated manganese reduction reactions were analyzed using a succession of X-ray spectroscopic measurements to assess the manganese phases consumed and formed throughout the reaction. Measuring the dynamics of manganese phase changes in real time is challenging because of the complex media necessary for microbial sustenance, the amorphous transient phases often formed in low-temperature reactions, and (during microbial experiments) the material complications introduced by cellular biomass. X-ray absorption spectroscopy (XAS) provides a valuable approach to probe the entire reaction sequence since XAS can focus on a given element (for e.g., Mn) without matrix effects and measure the coordination environment and redox state of all phases (contributing at least 5–

10% to the total Mn) regardless of crystallinity.[44] Real-time reduction experiments were performed and measured by XAS at the Stanford Synchrotron Radiation Lightsource, on either Beamline 11-2 or Beamline 4-1. We used high concentrations of Mn oxides and cells to have a strong Mn signal and rates sufficiently rapid to make experiments feasible in limited synchrotron time (i.e., < 12–14 h). The goal was not to mimic specific environments, but rather reveal how these different reduction reactions progress mechanistically.

Materials and Experimental Setup

To capture the reduction reaction in real-time, we set up an anaerobic flow-through system that siphoned a subsample of a stirred 1 L reaction vessel into a small flow cell wherein the X-ray beam could evaluate the Mn valence state and coordination environment (Figure 1). Our flow-through cell was constructed from polymethacrylate polymer using a 3D printer. Fluid moved rapidly (~1 mL s^{-1}) through anaerobic tubing and the flow-through cell. The reaction vessel contained 1 L of modified M1 minimal media (after Kostka and Nealson,[45] with phosphate eliminated unless noted) necessary for the biotic experiments, 20 mM lactate except in a lactate-limiting experiment, and began with freshly made colloidal Mn(IV)O_2 that manifested initially as colloids and often aggregated into larger clumps. Media was deoxygenated by bubbling prepure grade (99.998%) N_2 gas through the solution for 45 min[46] before sealing the 1–2 L bottle with a butyl rubber stopper.

For each experiment, we prepared ~6.3 mM colloidal MnO_2 by mixing equal weights of potassium permanganate and sodium thiosulfate (~1 g each, after Perez-Benito et al., 1989) in a small volume of Milli-Q water (~20 mL) and washed once with a dilute sodium chloride solution (8 mM NaCl) to remove any adsorbed sulfur species, pipetting away as much excess solution as possible. We added this colloidal MnO_2 to the reaction vessel in an anaerobic chamber. Colloidal MnO_2 substantially reduced the experimental time, since noncrystalline Mn(IV) oxides are much more reactive than crystalline Mn(IV) or Mn(III,IV) oxides such as pyrolusite or birnessite.[4] The media were titrated to pH 8, and adjusted using sodium hydroxide or hydrochloric acid after the addition of colloidal MnO_2 if necessary.

For the microbially mediated manganese reduction experiments, we used a wild-type bacterial system to most realistically capture the process dynamics of Mn reduction. We chose to use *S. oneidensis* MR-1 (hereafter referred to as MR-1), a well-studied model bacterium for understanding anaerobic metal reduction including the reduction of Mn(IV) oxides.[9,19,47,48] MR-1 employs either (or both) soluble 2-electron carriers (flavins)[49,50] or direct electron transfer at the cell surface[51–53] to pass electrons from a limited number of organic compounds to a substantial diversity of electron acceptors. Regardless of the mechanism, the overall reduction reaction produces dissolved inorganic carbon, alkalinity, and Mn(II), as in the reaction below, which should promote the precipitation of manganese carbonates.[25,54]

$$2\mathrm{Mn(IV)O_2} + \underset{\text{(lactate)}}{\mathrm{C_3H_5O_3^-}} + 4\mathrm{H^+} \rightleftharpoons 2\mathrm{Mn^{2+}} + \underset{\text{(acetate)}}{\mathrm{C_2H_3O_2^-}} + \mathrm{CO_2} + 3\mathrm{H_2O} \quad (1)$$

We grew MR-1 in conditions to optimize cellular density for expediency. MR-1 was grown aerobically in 1 L of Lysogeny Broth (LB) in a 25–30 ºC shaking incubator until the optical density at 600 nm was approximately 1.2. We then spun down the cells in 250 mL tubes using a centrifuge at 3000 rpm for 5 min and resuspended the cells in a small amount of LB. The cell paste (5–10 mL) was then added to the reaction vessel through the sampling port by a syringe after acquiring initial MnO_2 spectra. Multihour control experiments showed no evidence of beam reduction or reactions between lactate and Mn(IV) oxides in the absence of MR-1 (Supporting Information Figure S1).

We performed three experiments observing microbially mediated reduction of Mn(IV) oxides under endmember conditions and three experiments observing abiotic reduction of Mn(IV) oxides using common environmental reductants (Table 1). Microbial experiments varied between having added phosphate (4.3 mM) as a strong Mn(II) ligand, and either limited (1.5 mM in 3 allocations) or excess (20 mM) lactate. In abiotic experiments, we added either sodium sulfide (in small aliquots totaling ~5.25 mM of Na_2S) or ferrous chloride (aliquots totaling ~22 mM $FeCl_2$ for excess Fe^{2+} in complete reduction experiment) as a titrant to the manganese-(IV) oxide in the same media as the biotic experiments. Biological replicates of all experiments were performed either off-line, with the precipitate centrifuged and later analyzed by XAS as a powder monolayer on tape, or during additional real-time experiments at the synchrotron.

Synchrotron Data Acquisition and Analysis

X-ray absorption spectra through the Mn K-edge (acquisition time of ~20 min per scan) were measured throughout the experiment by XAS to detect Mn coordination and redox state (see refs 26 and 55–57). In the ferrous iron-induced reduction of manganese, X-ray absorption spectral parameters were adjusted to acquire X-ray absorption spectra at Fe K-edge in addition to the Mn K-edge, increasing the total measurement time to about 30 min per scan. Anaerobic conditions were maintained in the reaction vessel by nitrogen gas inflow. This experimental flow system was executed on both SSRL Beamlines 11-2 and 4-1, using a 50% detuned Si (220) double-crystal monochromator. The X-ray energy was calibrated using a $KMnO_4$ standard, setting the centroid of the pre-edge peak maximum to 6543.34 eV. Fluorescence data were obtained using either a 32 discrete element Canberra germanium detector (4-1) or a monolithic 100-element Canberra germanium detector (11-2) mounted at a 90º angle to the incident beam. Scatter was minimized using a 3-absorption length Cr filter and slits.

Particulate samples were collected approximately hourly using a sampling portal through the rubber stopper onto 2 μm Millipore filters and analyzed using synchrotron radiation X-ray diffraction (SR-XRD). SR-XRD was useful in these experiments, allowing us to take small subsamples at multiple time points without significantly affecting the reaction media. Filters were stored on sterile weigh boats and air-dried before characterizing crystalline products and confirming XAS identifications using SR-XRD on beamline 11-3. The majority of samples were measured 3–4 weeks after the experiments. We do not think oxidation of these materials postsampling was a problem because manganese oxidation is thermodynamically inhibited[58] and manganese carbonate powder mounts have previously been shown to be

stable on time scales greater than a week;[35] furthermore, there was no visual indication of oxidation (blackening) of the carbonate-dominated filters. SR-XRD was mainly useful to observe the ingrowth of rhodochrosite, as other phases were predominantly X-ray amorphous. Because colloidal $Mn(IV)O_2$ is poorly ordered,[59] similar to the biooxide δ-MnO_2,[60] no XRD pattern was seen in initial spectra. No XRD pattern was seen for another phase observed in XAS as well: a transient Mn(III) phase that did not appear in XRD patterns and therefore was either a soluble compound, a poorly ordered colloid, or otherwise X-ray amorphous. Data were compared to standards also analyzed by SR-XRD, and all data were calibrated on LaB_6 and integrated using the Area Diffraction Machine software suite.

XAS spectra were assessed using the SixPack software suite.[61] Mn and Fe XAS spectra were normalized using the background subtraction function on the SixPack software. In general, background subtraction was set to fit a Gaussian curve in the pre-edge from −150 eV to −50 eV before the edge, and the postedge was fit linearly from 50 to 300 eV past the edge; although during fitting, spectra were examined and adjusted individually to optimize normalization. Sequential spectra were grouped and averaged together if they appeared unchanged to increase the data quality (grouped spectra appear as bars and individual spectra appear as arrows beneath top panel in Figures 2 and 3). A 2-point averaging (smoothing) function was also applied to eliminate superficial noise in the spectra generated by the flow-through pump. The spectral sequence from each experiment, focusing on the near-edge region of XAS spectra from 6530 to 6590 eV, was analyzed using principal component analysis (PCA) in the SixPack module and, following Webb,[61] components were chosen as significant by examining the individual component *y*-axis ranges, the minimization of the IND functions, the ability for components to reconstruct a single experimental spectrum, and whether a time-progressive trend was formed in both component dimensions of score plots. Significant components were evaluated using the library analysis function in SixPack, wherein the vector space defined by these components is used to target transform a set of standards. Standards included reference compounds measured previously by the Fischer lab,[26] those published previously by Manceau et al.[55] and Bargar et al.,[28] and two additional Mn phosphate standards (hureaulite and reddingite) obtained for this study (Table S1). Internal experimental spectra (initial colloidal MnO_2 from the excess lactate experiment, dissolved Mn^{2+} from sulfide terminal spectra, and terminal spectra from excess phosphate and excess lactate experiments) were also made a part of the library to improve the quality of endmembers used in fitting routines. These are shown in Figure S2 alongside their most similar reference compounds. Spectra were chosen for use in Linear combination fitting by examining their Chi-squared, R, and SPOIL values (Table S1); in particular, spectra were eliminated as possible endmember components if their SPOIL values were >~6, following Webb[61] (with one exception discussed below).

We fit each experimental spectrum using PCA-chosen endmembers for each experiment and the Linear Combination least-squares fitting routine in SixPack software suite (Table S2). Component spectra were eliminated if they contributed less than 5% to the fit, except when the preceding and following fits included the spectra. Data spectra were only allowed to shift several tenths of an eV and initial Mn(IV) spectra from each experiment were used as the Mn(IV) component to improve the quality of fit and minimize the necessity for energy shifting from calibration drift. For consistency, the same endmember component spectra

were used in multiple experiments: for example, the feitknechtite standard from Manceau et al.[55] was preferred by target transform in high-lactate, sulfide, and iron experiments and thus was used in the lactate-limited experiment spectral fits rather than the feitknechtite standard obtained from Bargar[28] even though library analysis of this experiment preferred the latter spectrum. The iron-induced reduction experimental spectra were grouped together for PCA and target transform analyses because there were very few spectra for complete iron and limited iron reduction experiments. Furthermore, regardless of number or concentration of iron additions, the reaction endmember components should be the same for both experiments. Errors on component fraction estimates using linear combination least-squares fitting are typically ~10%.

Manganese Solution Data

Replicate experiments were performed to obtain estimates of solution concentrations of Mn^{2+} throughout the endmember experiments (high-phosphate and MR-1, high-lactate and MR-1, and ferrous-iron-induced and sulfide-induced Mn(IV) reductions). Small samples (1.5 mL) were extracted from the reaction media using syringes and immediately centrifuged for 5–10 min. Approximately 1 mL of the supernatant was removed and placed into a new Eppendorf tube. Twenty μL was then taken from the supernatant and diluted into 13 mL of 2% nitric acid for measurement by inductively coupled plasma mass spectrometry (ICP-MS) in the Caltech Environmental Analysis Center. These experiments were either performed in an anaerobic chamber or supernatant samples were immediately diluted into acid, to prevent Mn(II) oxidation in solution samples. Samples on the ICP-MS were bracketed by blanks and Mn(II) standards every ~12 samples, and Mn(II) concentrations were calculated by interpolating between in-house Mn(II) calibration standards.

RESULTS AND DISCUSSION

Biological Experimental Results

We varied phosphate and lactate concentrations during Mn-reduction by *S. oneidensis* MR-1 to test how these conditions might affect the transient phases and products of microbial respiration of manganese oxides. Mn(II)-phosphates are highly insoluble precipitates (K_{sp} of $Mn(II)_3(PO_4)_2$ and $MnHPO_4$ are $10^{-23.8}$ and $10^{-12.9}$, respectively[62]), and so a high-phosphate environment has the advantage of trapping much of the produced Mn^{2+}. In this high-phosphate experiment, we observed a direct transformation of MnO_2 into a Mn(II)-phosphate phase with a spectrum similar to a hureaulite ($Mn^{2+}_5(PO_3OH)_2(PO_4)_2{\cdot}4H_2O$) standard (Figure 2a; Figure S2; Figure S3; Table S2). Isosbestic points—energies where all spectra have the same absorbance—are seen in two-phase conversions[28] and these points were clearly observed in the data from high phosphate experiments (see Figure 2a inset). PCA analyses (see Materials and Methods) confirmed that there are only two significant components that fit these spectra, and library target transforms of aqueous Mn^{2+} and various forms of Mn(III) oxyhydroxides, Mn(III) organic complexes, and Mn(III) phosphate complexes have SPOIL values >9, signifying these are unacceptable endmembers for fitting routines[61] (Table S1). Therefore, there were no transitional Mn(III) mineral phases or reaction intermediates observed within the time resolution of the experiments (20 min) and above the limit of detection (5–10% of the total Mn concentration). Under these high

phosphate concentrations, the Mn(II) produced via microbial reduction was predominantly precipitated as a Mn(II)-phosphate salt. The pH measurements confirmed this relatively simple reaction: the respiration of MnO_2 consumed protons (Reaction 1) and the pH initially rose, but then the system was quickly stabilized as Mn(II)-phosphate formed with little subsequent change to the pH (Figure 2a). Solution analyses demonstrated that, after microbial respiration of Mn(IV) oxides commenced, there were low levels of aqueous Mn^{2+} that reached a maximum of ~230–250 μM at 2–3 h and then this dissolved Mn(II) dropped to ~100 μM as the reaction completed (Table S3). These Mn^{2+} concentrations, not discernible by XAS analyses, constituted a very small portion (<4%) of the ~6 mM Mn(IV) oxides present in the initial solution, likely representing the equilibrium between soluble or phosphate-complexed Mn^{2+} and Mn(II)-phosphate salts.

In contrast, the two experiments with negligible phosphate had dramatically different reaction progressions and products. The lactate-replete (20 mM) experiment provided a measure of what occurs in environments where manganese oxides are limiting—conditions that can be compared to highly productive coastal settings with large relative fluxes of organic matter.[63,64] Although the experiment began without the high inorganic carbon present in the ocean, the system quickly gained inorganic carbon as lactate oxidation by MR-1 proceeded. This high-lactate experiment showed several important transient phases, including a Mn(III) phase and Mn^{2+} in solution, before finally precipitating a crystalline rhodochrosite ($MnCO_3$) product (Figure 2b; Figures S4, S5). The Mn(III) transient phase appeared as a ruddy brown solid, quite distinct from the initial black Mn(IV) oxides (see filter photos in Figure S5), and PCA target transform routines (see Materials and Methods) chose a Mn(III)-oxyhydroxide, feitknechtite (β-MnOOH), as a component of this spectral suite in addition to Mn(IV) oxides, aqueous Mn^{2+}, and an internal rhodochrosite spectra (Table S1). Mn(III)-organic complex reference compounds (Mn(III)-phthalocyanine chloride, Mn(III)-acetyl acetonate, Mn(III)-tetra(4-pyridyl)porphine chloride) and Mn(III)-phosphate reference compounds had unacceptable SPOIL values to be potential components of this experiment (Table S1). Linear combination fitting of sequence spectra revealed a gradual decrease in Mn(IV) oxides and increase in feitknechtite and aqueous Mn^{2+}, and feitknechtite appeared to occur at free Mn^{2+} concentrations of several hundred micromolar (Figure 2b, Table S2). Spectra and solution data both indicated that aqueous Mn^{2+} reached high levels, over 80% of the spectral signal and up to ~1 mM, similar to maximum levels measured in iron and sulfide experiments. As this is only ~16% of Mn present in the system, a majority of the Mn(II) was likely associated with the particles still present. Rhodochrosite began to appear after Mn^{2+} comprised >80% of the spectral signal (Table S2, Figure 2b) and eventually became the sole crystalline product (Figure 2b, Figure S5). Similar to the phosphate precipitates, there was apparent equilibrium between rhodochrosite and aqueous Mn^{2+} even at the time the final spectrum was taken. Whereas the final seven spectra from this experiment showed little change, they were best fit by 27% aqueous Mn^{2+} and 73% of a rhodochrosite standard (labeled $Rh+Mn_{aq}$). The pH changes throughout the experiment reflected the various reactions that occurred. The pH continued to rise past the maximum in Figure 2a (~8.35) all the way up to ~8.6, and then it dropped rapidly followed by a slow decrease approximately back to its original pH of 8. This pH drop marked the precipitation of rhodochrosite ($MnCO_3$).

$$Mn^{2+} + CO_2 + H_2O \rightleftharpoons MnCO_3 + 2H^+ \quad (2)$$

A third biological reduction experiment with minimal phosphate had an additional limitation in its organic carbon (lactate) source relative to manganese oxides—conditions more comparable to an oligotrophic open-ocean marine setting with low primary productivity and organic carbon fluxes,[63,64] although again without initial inorganic carbon present. This experiment displayed the production of aqueous Mn^{2+} and a Mn(III) phase similar to the transient Mn(III) phase observed in the high-lactate experiments—best fit by a feitknechtite component (Figure 2c, Table S1). The media began with just 0.5 mM lactate, and we then successively added two more aliquots of 0.5 mM lactate, totaling 1.5 mM lactate consumed. The initial conditions yielded minimal changes, but the fit was optimized in t1 and t2 spectra by including a fraction of feitknechtite (22–26%) and aqueous Mn^{2+} (10–14%) (Table S2). Further addition of lactate led to a redox state system stabilized as 43% Mn(IV), 20% feitknechtite, and 37% aqueous Mn^{2+} (shown in t4, Figure 2c; Table S2). Spectra were similar for approximately an hour before we added a third aliquot of lactate, and this prompted rapid change followed by a stasis in both pH and spectral fingerprint. The system became dominated by Mn^{2+} but feitknechtite and Mn(IV) were still present at 25% and 14% of the total Mn, respectively. Our spectral measurements indicated that no redox changes were observed without addition of the designated reductant, suggesting that the Mn(III) oxyhydroxide phase could have been stable over much longer time scales. The development of three distinct stable redox states was observed in the unchanging pH plateaus (Figure 2c).

Mechanism of Biological Mn(IV) Reduction

Mn(IV) reduction by bacteria such as MR-1 has generally been measured and presented as a 2-electron reaction going from Mn(IV) to Mn(II) (e.g., see ref 33), but recent reports suggest Mn(III) intermediates may form during this process.[19,20] The absence of observable Mn(III) oxyhydroxide solids in our high-phosphate experiments is revealing of the underlying redox mechanism of Mn(IV) reduction by MR-1. The formation of a Mn(III) solid phase and its subsequent bioreduction in the low-phosphate experiments was easily observed by the discrete 20-min time frame of our spectral sequences, and this brown solid appears to be best fit by feitknechtite. The fact that no long-lived Mn(III) phase was observed under high-phosphate conditions suggests that this feitknechtite was not produced from a one-electron transfer by MR-1. Low levels of manganese undetectable by our methods (<5–10% of total Mn) could have been present as complexed Mn(III) species formed as intermediates during the reduction reaction. However, our results demonstrate that no major Mn(III) phase is produced by Mn(IV) reduction by MR-1. Either MR-1 performs a direct 2-electron transfer to solid Mn(IV) oxides and releases aqueous Mn^{2+}, or MR-1 reduces Mn(IV) oxides via rapid biologically mediated electron transfer in 2 single-electron steps, proceeding through a low-concentration, highly reactive Mn(III) intermediate before producing Mn^{2+}. The latter mechanism would be consistent with recent results suggesting Mn(IV) reduction proceeds through a soluble Mn(III) intermediate that comprises <4% of the total Mn.[19] The former option could be mediated by soluble flavins[50] (two-electron carriers) facilitating Mn(IV) reduction to Mn^{2+}.

Abiotic Mn(IV) Reduction Experimental Results

Abiotic reduction experiments using inorganic titrants also formed a Mn(III) phase, but the final Mn(II) products observed were distinct from biological respiration experiments. Both sulfide (Figure 3a) and Fe^{2+} (Figure 3b,c) titration experiments produced a Mn(III) phase similar to low-phosphate biological reduction experiments, best fit in PCA analyses by feitknechtite. The sul3de-induced reduction spectral sequence showed this transient phase especially clearly due to the very gradual additions of sulfide. A limited-iron addition experiment (Figure 3c) indicated this Mn(III) oxyhydroxide phase can be stabilized with limited reductant, similar to our lactate-limiting experiment. In the experiments with Fe^{2+} additions, iron was oxidized in less than the time scale of a single Mn–Fe scan through the K-edge (<30 min) (Figure S6), and the iron oxide phase produced closely matched our lepidocrocite (α-FeOOH) standard in XAS and SR-XRD (Figures S6, S7). With excess reductant, however, both abiotic experiments formed aqueous Mn^{2+} without any mineral products (Figure 3a,b). High levels of soluble Mn(II) were also observed in solution data from replicate experiments, which reached at least ~1 to 2 mM Mn^{2+} (Table S3). No carbonates were observed in the abiotic experiments because dissolved inorganic carbon was neither present nor produced, unlike the dissolved inorganic carbon generated by lactate oxidation in our biological experiments.

These results are somewhat artificial, especially in the case of sulfide-induced manganese reduction, which would be expected to produce Mn-carbonate in environments with abundant dissolved inorganic carbon such as seawater. This is consistent with previous work that has noted reactions between sulfide and Mn(IV) oxides producing rhodochrosite.[38–41] These other reports were all in natural sediments with active microbial cycling and respiration,[39] in experiments with microbes performing thiosulfate or sulfur disproportionation in the presence of Mn(IV) oxides,[38] or with concomitant microbial manganese oxide reduction and either sulfate or thiosulfate reduction.[40,41] All of these environments would have high dissolved inorganic carbon, as well as elevated alkalinity from microbially mediated reduction reactions—conditions that promote the precipitation of carbonates like rhodochrosite. Thus, in abiotic experiments supplemented with dissolved inorganic carbon, reactions between sulfide and Mn(IV) oxides should produce Mn(II)-carbonates.

The lack of diagenetically stable manganese carbonate in the Fe^{2+} addition experiments is more likely a typical outcome in sedimentary environments with low dissolved inorganic carbon because the reaction between Mn oxides and Fe^{2+} consumes alkalinity. Mn^{2+} remains highly soluble at low to neutral pH, and so the acidity generated due to the hydrolysis and precipitation of ferric oxide during reduction of Mn(IV) oxides should stabilize the aqueous Mn^{2+} produced in these experiments and Mn(II)-carbonate (or Mn(II)-hydroxide) precipitation will not be promoted (Figure 3b,c). Aqueous Mn^{2+} could diffuse or be advected away from the reaction substrates and would not accumulate in the sediments (or produce a geologically observable manganese deposit). However, in well-buffered systems with sufficient inorganic carbon and very high degrees of supersaturation of carbonate phases, Fe^{2+}-mediated reduction of Mn(IV) oxides may still produce small amounts of Mn-carbonate.

Significance of Mn(III) Phase

A notable phase observed in both abiotic experiments and during the respiration of Mn(IV) oxides by MR-1 was a Mn(III) oxyhydroxide, that appeared both as a transient phase during the reaction sequence and as a product when the reductant (ferrous iron or lactate) was limiting (Figures 2c, 3c). It appears from comparing biological experiments with and without phosphate that feitknechtite is a secondary phase unrelated to Mn(IV) reduction mediated by MR-1. Because of the lack of Mn(III) and low Mn^{2+} concentrations in the high-phosphate microbial reduction experiments, we hypothesize that Mn(III) oxyhydroxides in low-phosphate microbial experiments are a secondary transient phase, forming as the result of the presence of significant aqueous Mn^{2+}. An attractive mechanism for the formation of Mn(III) oxyhydroxides using Mn^{2+} may be comproportionation reactions studied in previous work,[60,65,66] where produced Mn^{2+} can reduce remnant Mn(IV) oxides, as in Reaction 3.

$$Mn^{2+} + Mn(IV)O_2 + 2H_2O \rightleftharpoons 2Mn(III)OOH + 2H^+ \quad (3)$$

In high-lactate experiments, feitknechtite was observed spectrally from the first time point after cells were added until approximately 4 h after cells were added, as pH rose to ~8.6 and returned to ~8.4 (Figure 2b). Solution data at these pHs in a replicate experiment suggest that free Mn^{2+} ranged from ~300 μM to 1 mM (Table S3), although these concentrations are likely low estimates as the amount of Mn(II) adsorbed to solids was not measured. This is consistent with previous reports that suggest feitknechtite is produced from Mn(IV) oxides when they are in the presence of ~500 μM or greater of Mn(II).[60,66] Experiments under anoxic conditions have determined that this reaction in the Mn(III,IV) oxide birnessite is the result of interfacial electron transfer to structural Mn(IV) atoms from adsorbed Mn(II), followed by the transformation of product Mn(III) into Mn(III)OOH.[65] It is probable that colloidal $Mn(IV)O_2$ reacts similarly to birnessite, and therefore the feitknechtite observed in low-phosphate MR-1 respiration of Mn(IV) oxides was likely produced in an analogous fashion.

Feitknechtite was also observed in our abiotic ferrous iron and sulfide experiments, but the formation mechanism of the MnOOH in these experiments is less well constrained. Previous experiments studying reactions between Mn(IV) oxides and sulfide or ferrous iron presented evidence of short-lived Mn(III) intermediates, captured by Mn(III) ligands such as pyrophosphate or siderophores.[20,67,68] However, these putative Mn(III) intermediates are extremely difficult to detect in reactions with sulfide, even by powerful UV–vis and voltammetry techniques;[69] additionally, Mn(III) is reduced by ferrous iron and sulfide in seconds[70] unless strong Mn(III) ligands are present.[71] Despite evidence for two single-electron transfers to the Mn(IV) surface, these steps appear to be extremely rapid — occurring in seconds[67,72]— and the reported product of Mn(IV) reduction by iron and sulfide without strong Mn(III) ligands present is aqueous Mn^{2+}.[67,69] It is possible the brief Mn(III) intermediates in these reactions can undergo hydration and form a temporary MnOOH compound; however, we think that the short-lived Mn(III) intermediates reported in

earlier works would have been undetected in our experiments. The feitknechtite observed in the Fe^{2+} and sulfide addition experiments, comprising 10–30% of the total spectral signal for most of transitional spectra between Mn(IV) and Mn^{2+}, was more likely formed by comproportionation reactions, analogous to the mechanism inferred from the mineral sequence in the low-phosphate biological experiments.

Importantly, this Mn(III) oxyhydroxide is a phase that could potentially enter the sedimentary record, as long as the pore fluids were sufficiently limiting in electron donors such as sulfide, ferrous iron, and organic matter (e.g., see the final assemblages in Figures 2c, 3c). Feitknechtite has been demonstrated to be stable until Mn(II) concentrations are reduced to submicromolar levels.[60] Alternatively, other experiments have shown that feitknechtite transforms into manganite (a polymorph of feitknechtite) with aging,[65,66] and this manganite can remain stable for at least a year.[66] In general, manganite is much more stable than feitknechtite[73] and thus may form a preservable precursor to Mn(III) phases commonly observed in the rock record.

Braunite is a prominent Mn(III) phase found in major manganese deposits throughout the rock record,[24,26] but neither its process of formation nor its precursor phases are known. One of the proposed pathways of braunite formation involves reacting a Mn(III) oxide, such as Mn_2O_3, with silica (aqueous SiO_2 or H_4SiO_4),[26,74] and the Mn(III) oxyhydroxide phase produced in our experiments may be an appealing preliminary phase for this reaction. In the rock record, braunite co-occurs with Mn(II)-carbonates,[26,75] which, according to our experiments, is consistent with the hypothesis that this Mn(III,II) assemblage observed in several ore-forming manganese deposits could reflect the microbial reduction of precursor sedimentary Mn(IV) oxides. Conservatively, the presence of braunite and Mn(II)-carbonates in ancient rocks can be interpreted to indicate a manganese oxide-rich precursor sediment that was limiting in electron donors and replete with inorganic carbon, and likely was undergoing cycling of carbon and/or sulfur.

Interpreting Experimental Results

The experimental data presented here highlight the complex interactions and pathways that can alter Mn(IV) oxides into a variety of secondary and tertiary phases. While future work might focus on constraining reactions under conditions more similar to sedimentary or soil porewater conditions, we can nevertheless conclude several valuable results based on the experimental data presented here. Three phases were produced that can be potential long-lived markers of environmental conditions and possible microbial involvement. Manganese(II)-phosphates, manganese(II)-carbonates, and manganese(III)-oxyhydroxides are all insoluble precipitates that are either already crystalline or could age into minerals such as hureaulite, reddingite, rhodochrosite, kutnohorite, and manganese(III) phases such as Mn(III) oxides (bixbyite, Mn_2O_3) or even braunite. Each of these has differing requirements in terms of the balance of electron donor compared to electron acceptor, inorganic carbon and alkalinity, and other environmental conditions (such as high phosphate concentrations) that promote the stability of these three phases (see Abstract Graphic). With continued effort to constrain the reaction transient and product solids for different reduction pathways, it will be possible to leverage these measurements against minerals found in

Earth's modern sediments and ancient rock record to add a more nuanced environmental and process-based understanding to geological observations.

Supplementary Material

Refer to Web version on PubMed Central for supplementary material.

Acknowledgments

We express our gratitude to Cynthia Patty, John Bargar, Courtney Roach, and Cathy Knotts for going above and beyond so that it was possible for us to run these experiments at the synchrotron; to Jeffrey Gralnick, Annie Rowe, Kyle Metcalfe, Kevin Sutherland, and Jim Hemp for experimental assistance and advice; to Nathan Dalleska for invaluable assistance acquiring data on the ICP-MS; and to George Rossman for assistance with and frequent access to his RAMAN and Fourier Transform Infrared Spectrometer. We also thank Alex Sessions, Dianne Newman, Victoria Orphan, Julie Cosmidis, and four anonymous reviewers for very helpful manuscript feedback. We acknowledge a Packard Foundation grant to W.W.F., which funded much of this research, an NSF Graduate Research Fellowship (DGE-1144469) to J.E.J., and a NASA Astrobiology Institute (NAI) grant that supported K.H.N. and P.S. Portions of this research were carried out at the Stanford Synchrotron Radiation Lightsource, SLAC National Accelerator Laboratory, which is supported by the U.S. Department of Energy, Office of Science, Office of Basic Energy Sciences under Contract DE-AC02-76SF00515. The SSRL Structural Molecular Biology Program is supported by the DOE Office of Biological and Environmental Research, and by the National Institutes of Health, National Institute of General Medical Sciences (including P41GM103393). The contents of this publication are solely the responsibility of the authors and do not necessarily represent the official views of NIGMS or NIH.

References

1. Tebo BM, Johnson HA, McCarthy JK, Templeton AS. Geomicrobiology of manganese(II) oxidation. Trends Microbiol. 2005; 13(9):421–428. [PubMed: 16054815]
2. Lovley DR, Phillips EJP. Novel Mode of Microbial Energy Metabolism: Organic Carbon Oxidation Coupled to Dissimilatory Reduction of Iron or Manganese. Appl Environ Microbiol. 1988; 54(6): 1472–1480. [PubMed: 16347658]
3. Myers CR, Nealson KH. Bacterial manganese reduction and growth with manganese oxide as the sole electron acceptor. Science. 1988; 240(4857):1319–1321. [PubMed: 17815852]
4. Burdige DJ, Dhakar SP, Nealson KH. Effects of manganese oxide mineralogy on microbial and chemical manganese reduction. Geomicrobiol J. 1992; 10(1):27–48.
5. Van Cappellen P, Viollier E, Roychoudhury A, Clark L, Ingall E, Lowe K, Dichristina T. Biogeochemical Cycles of Manganese and Iron at the Oxic-Anoxic Transition of a Stratified Marine Basin (Orca Basin, Gulf of Mexico). Environ Sci Technol. 1998; 32(19):2931–2939.
6. Canfield DE, Thamdrup B, Hansen JW. The anaerobic degradation of organic matter in Danish coastal sediments: Iron reduction, manganese reduction, and sulfate reduction. Geochim Cosmochim Acta. 1993; 57(16):3867–3883. [PubMed: 11537734]
7. Thamdrup B, Rosselló-Mora R, Amann R. Microbial Manganese and Sulfate Reduction in Black Sea Shelf Sediments. Appl Environ Microbiol. 2000; 66(7):2888–2897. [PubMed: 10877783]
8. Burdige DJ, Nealson KH. Chemical and microbiological studies of sulfide-mediated manganese reduction. Geomicrobiol J. 1986; 4(4):361–387.
9. Myers CR, Nealson KH. Microbial reduction of manganese oxides: Interactions with iron and sulfur. Geochim Cosmochim Acta. 1988; 52(11):2727–2732.
10. Ying SC, Kocar BD, Griffis SD, Fendorf S. Competitive Microbially and Mn Oxide Mediated Redox Processes Controlling Arsenic Speciation and Partitioning. Environ Sci Technol. 2011; 45(13):5572–5579. [PubMed: 21648436]
11. Fredrickson JK, Zachara JM, Kennedy DW, Liu C, Duff MC, Hunter DB, Dohnalkova A. Influence of Mn oxides on the reduction of uranium(VI) by the metal-reducing bacterium Shewanella putrefaciens. Geochim Cosmochim Acta. 2002; 66(18):3247–3262.

12. Thamdrup B, Finster K, Hansen JW, Bak F. Bacterial Disproportionation of Elemental Sulfur Coupled to Chemical Reduction of Iron or Manganese. Appl Environ Microbiol. 1993; 59(1):101–108. [PubMed: 16348835]
13. Thamdrup B, Glud RN, Hansen JW. Manganese oxidation and in situ manganese fluxes from a coastal sediment. Geochim Cosmochim Acta. 1994; 58(11):2563–2570.
14. van Cappellen P, Wang Y. Cycling of iron and manganese in surface sediments; a general theory for the coupled transport and reaction of carbon, oxygen, nitrogen, sulfur, iron, and manganese. Am J Sci. 1996; 296(3):197–243.
15. Wang, Z., Giammar, DE. Advances in the Environmental Biogeochemistry of Manganese Oxides. Vol. 1197. ACS Symposium Series; American Chemical Society; Washington, DC: 2015. Metal Contaminant Oxidation Mediated by Manganese Redox Cycling in Subsurface Environment; p. 29-50.
16. Dick GJ, Clement BG, Webb SM, Fodrie FJ, Bargar JR, Tebo BM. Enzymatic microbial Mn(II) oxidation and Mn biooxide production in the Guaymas Basin deep-sea hydrothermal plume. Geochim Cosmochim Acta. 2009; 73:6517–6530.
17. Fuller CC, Harvey JW. Reactive Uptake of Trace Metals in the Hyporheic Zone of a Mining-Contaminated Stream, Pinal Creek, Arizona. Environ Sci Technol. 2000; 34(7):1150–1155.
18. Tebo, BM., Rosson, RA., Nealson, KH. Potential for manganese(II) oxidation and manganese(IV) reduction to co-occur in the anoxic non-sulfidic zone of the Black Sea. In: Izdar, E., Murray, JW., editors. Black Sea Oceanography. Kluwer Academic Publishers; Dordrecht, The Netherlands: 1991. p. 173-185.
19. Lin H, Szeinbaum NH, DiChristina TJ, Taillefert M. Microbial Mn(IV) reduction requires an initial one-electron reductive solubilization step. Geochim Cosmochim Acta. 2012; 99:179–192.
20. Madison AS, Tebo BM, Mucci A, Sundby B, Luther GW. Abundant Porewater Mn(III) Is a Major Component of the Sedimentary Redox System. Science. 2013; 341(6148):875–878. [PubMed: 23970696]
21. Froelich PN, Klinkhammer GP, Bender ML, Luedtke NA, Heath GR, Cullen D, Dauphin P, Hammond D, Hartman B, Maynard V. Early oxidation of organic matter in pelagic sediments of the eastern equatorial Atlantic: suboxic diagenesis. Geochim Cosmochim Acta. 1979; 43(7):1075–1090.
22. Nealson KH, Saffarini D. Iron and Manganese in Anaerobic Respiration: Environmental Significance, Physiology, and Regulation. Annu Rev Microbiol. 1994; 48(1):311–343. [PubMed: 7826009]
23. Roy S. Sedimentary manganese metallogenesis in response to the evolution of the Earth system. Earth-Sci Rev. 2006; 77(4):273–305.
24. Maynard JB. The Chemistry of Manganese Ores through Time: A Signal of Increasing Diversity of Earth-Surface Environments. Econ Geol Bull Soc Econ Geol. 2010; 105(3):535–552.
25. Calvert SE, Pedersen TF. Sedimentary geochemistry of manganese; implications for the environment of formation of manganiferous black shales. Econ Geol Bull Soc Econ Geol. 1996; 91(1):36–47.
26. Johnson JE, Webb SM, Ma C, Fischer WW. Manganese mineralogy and diagenesis in the sedimentary rock record. Geochim Cosmochim Acta. 2016; 173:210–231.
27. Webb SM, Tebo BM, Bargar JR. Structural characterization of biogenic Mn oxides produced in seawater by the marine bacillus sp. strain SG-1. Am Mineral. 2005; 90(8–9):1342–1357.
28. Bargar JR, Tebo BM, Villinski JE. In situ characterization of Mn(II) oxidation by spores of the marine Bacillus sp. strain SG-1. Geochim Cosmochim Acta. 2000; 64:2775–2778.
29. Murray JW, Dillard JG, Giovanoli R, Moers H, Stumm W. Oxidation of Mn(II): Initial mineralogy, oxidation state and ageing. Geochim Cosmochim Acta. 1985; 49(2):463–470.
30. Wehrli, B., Friedl, G., Manceau, A. Aquatic Chemistry; Advances in Chemistry. Vol. 244. American Chemical Society; Washington, DC: 1995. Reaction Rates and Products of Manganese Oxidation at the Sediment-Water Interface; p. 111-134.
31. McKeown DA, Post JE. Characterization of manganese oxide mineralogy in rock varnish and dendrites using X-ray absorption spectroscopy. Am Mineral. 2001; 86(5–6):701–713.

32. Tebo BM, Bargar JR, Clement BG, Dick GJ, Murray KJ, Parker D, Verity R, Webb SM. BIOGENIC MANGANESE OXIDES: Properties and Mechanisms of Formation. Annu Rev Earth Planet Sci. 2004; 32(1):287–328.
33. De Schamphelaire L, Rabaey K, Boon N, Verstraete W, Boeckx P. Minireview: The Potential of Enhanced Manganese Redox Cycling for Sediment Oxidation. Geomicrobiol J. 2007; 24(7–8): 547–558.
34. Coleman ML, Fleet A, Donson P. Preliminary Studies of Manganese-Rich Carbonate Nodules from Leg 68, Site 503, Eastern Equatorial Pacific. Init Repts DSDP. 1982; 68:481–489.
35. Johnson JE, Webb SM, Thomas K, Ono S, Kirschvink JL, Fischer WW. Manganese-oxidizing photosynthesis before the rise of cyanobacteria. Proc Natl Acad Sci U S A. 2013; 110(28):11238–11243. [PubMed: 23798417]
36. Tsikos H, Beukes NJ, Moore JM, Harris C. Deposition, Diagenesis, and Secondary Enrichment of Metals in the Paleoproterozoic Hotazel Iron Formation, Kalahari Manganese Field, South Africa. Econ Geol Bull Soc Econ Geol. 2003; 98(7):1449–1462.
37. Okita PM, Maynard JB, Spiker EC, Force ER. Isotopic evidence for organic matter oxidation by manganese reduction in the formation of stratiform manganese carbonate ore. Geochim Cosmochim Acta. 1988; 52(11):2679–2685.
38. Böttcher ME, Thamdrup B. Anaerobic sulfide oxidation and stable isotope fractionation associated with bacterial sulfur disproportionation in the presence of MnO2. Geochim Cosmochim Acta. 2001; 65(10):1573–1581.
39. Meister P, Bernasconi SM, Aiello IW, Vasconcelos C, Mckenzie JA. Depth and controls of Ca-rhodochrosite precipitation in bioturbated sediments of the Eastern Equatorial Pacific, ODP Leg 201, Site 1226 and DSDP Leg 68, Site 503. Sedimentology. 2009; 56(5):1552–1568.
40. Huckriede H, Meischner D. Origin and environment of manganese-rich sediments within black-shale basins. Geochim Cosmochim Acta. 1996; 60(8):1399–1413.
41. Lee JH, Kennedy DW, Dohnalkova A, Moore DA, Nachimuthu P, Reed SB, Fredrickson JK. Manganese sulfide formation via concomitant microbial manganese oxide and thiosulfate reduction. Environ Microbiol. 2011; 13(12):3275–3288. [PubMed: 21951417]
42. Fischer TB, Heaney PJ, Jang JH, Ross DE, Brantley SL, Post JE, Tien M. Continuous time-resolved X-ray diffraction of the biocatalyzed reduction of Mn oxide. Am Mineral. 2008; 93(11–12):1929–1932.
43. Venkateswaran K, Moser DP, Dollhopf ME, Lies DP, Saffarini DA, MacGregor BJ, Ringelberg DB, White DC, Nishijima M, Sano H, et al. Polyphasic taxonomy of the genus Shewanella and description of Shewanella oneidensis sp. nov. Int J Syst Bacteriol. 1999; 49(2):705–724. [PubMed: 10319494]
44. Brown GE, Sturchio NC. An Overview of Synchrotron Radiation Applications to Low Temperature Geochemistry and Environmental Science. Rev Mineral Geochem. 2002; 49(1):1–115.
45. Kostka, J., Nealson, KH. Isolation, Cultivation and Characterization of Iron- and Manganese-Reducing Bacteria. In: Burlage, RS.Atlas, R.Stahl, D.Geesey, G., Sayler, G., editors. Techniques in Microbial Ecology. Oxford University Press; Oxford: 1998. p. 468
46. Butler IB, Schoonen MAA, Rickard DT. Removal of dissolved oxygen from water: A comparison of four common techniques. Talanta. 1994; 41(2):211–215. [PubMed: 18965910]
47. Richardson DJ, Butt JN, Fredrickson JK, Zachara JM, Shi L, Edwards MJ, White G, Baiden N, Gates AJ, Marritt SJ, et al. The “porin-cytochrome” model for microbe-to-mineral electron transfer. Mol Microbiol. 2012; 85(2):201–212. [PubMed: 22646977]
48. Harris HW, El-Naggar MY, Bretschger O, Ward MJ, Romine MF, Obraztsova AY, Nealson KH. Electrokinesis is a microbial behavior that requires extracellular electron transport. Proc Natl Acad Sci U S A. 2010; 107(1):326–331. [PubMed: 20018675]
49. Marsili E, Baron DB, Shikhare ID, Coursolle D, Gralnick JA, Bond DR. Shewanella secretes flavins that mediate extracellular electron transfer. Proc Natl Acad Sci U S A. 2008; 105(10): 3968–3973. [PubMed: 18316736]
50. Kotloski NJ, Gralnick JA. Flavin electron shuttles dominate extracellular electron transfer by Shewanella oneidensis. mBio. 2013; 4(1):1–4.

51. Gorby YA, Yanina S, McLean JS, Rosso KM, Moyles D, Dohnalkova A, Beveridge TJ, Chang IS, Kim BH, Kim KS, et al. Electrically conductive bacterial nanowires produced by Shewanella oneidensis strain MR-1 and other microorganisms. Proc Natl Acad Sci U S A. 2006; 103(30): 11358–11363. [PubMed: 16849424]
52. Myers CR, Myers JM. Localization of cytochromes to the outer membrane of anaerobically grown Shewanella putrefaciens MR-1. J Bacteriol. 1992; 174(11):3429–3438. [PubMed: 1592800]
53. Okamoto A, Hashimoto K, Nealson KH, Nakamura R. Rate enhancement of bacterial extracellular electron transport involves bound flavin semiquinones. Proc Natl Acad Sci U S A. 2013; 110(19): 7856–7861. [PubMed: 23576738]
54. Bergmann KD, Grotzinger JP, Fischer WW. Biological Influences on Seafloor Carbonate Precipitation. Palaios. 2013; 28(2):99–115.
55. Manceau A, Marcus MA, Grangeon S. Determination of Mn valence states in mixed-valent manganates by XANES spectroscopy. Am Mineral. 2012; 97:816–827.
56. Bargar JR, Webb SM, Tebo BM. Structural Determination of Marine Bacteriogenic Manganese Oxides. SSRL Sci Highlight. 2005:1–4.
57. Webb SM, Dick GJ, Bargar JR, Tebo BM. Evidence for the presence of Mn(III) intermediates in the bacterial oxidation of Mn(II). Proc Natl Acad Sci U S A. 2005; 102(15):5558–5563. [PubMed: 15800042]
58. Luther GWI. The Role of One- and Two-Electron Transfer Reactions in Forming Thermodynamically Unstable Intermediates as Barriers in Multi-Electron Redox Reactions. Aquat Geochem. 2010; 16(3):395–420.
59. Morgan JJ, Stumm W. Colloid-chemical properties of manganese dioxide. J Colloid Sci. 1964; 19(4):347–359.
60. Bargar JR, Tebo BM, Bergmann U, Webb SM, Glatzel P, Chiu VQ, Villalobos M. Biotic and abiotic products of Mn(II) oxidation by spores of the marine Bacillus sp. strain SG-1. Am Mineral. 2005; 90(1):143–154.
61. Webb SM. SIXpack: a graphical user interface for XAS analysis using IFEFFIT. Phys Scr. 2005; 2005(T115):1011.
62. Ball, JW., Nordstrom, DK. Open-File Report; USGS Numbered Series 90–129. 1991. WATEQ4F -- User's manual with revised thermodynamic data base and test cases for calculating speciation of major, trace and redox elements in natural waters.
63. Conkright, ME., Garcia, HE., O'Brien, TD., Locarnini, RA., Boyer, TP., Antonov, CS. World Ocean Atlas 2001. In: Levitus, E., editor. NOAA Atlas NESDIS 52. Vol. 4. U.S. Gov. Printing Office; Washington, DC: 2002. Nutrients
64. Williams, RG., Follows, MJ. Ocean Dynamics and the Carbon Cycle: Principles and Mechansims. Cambridge University Press; New York: 2011.
65. Elzinga EJ. Reductive Transformation of Birnessite by Aqueous Mn(II). Environ Sci Technol. 2011; 45(15):6366–6372. [PubMed: 21675764]
66. Mandernack KW, Post J, Tebo BM. Manganese mineral formation by bacterial spores of the marine Bacillus, strain SG-1: Evidence for the direct oxidation of Mn(II) to Mn(IV). Geochim Cosmochim Acta. 1995; 59(21):4393–4408.
67. Siebecker M, Madison AS, Luther GW III. Reduction Kinetics of Polymeric (Soluble) Manganese (IV) Oxide (MnO2) by Ferrous Iron (Fe2+). Aquat Geochem. 2015; 21(2–4):143–158.
68. Nico PS, Zasoski RJ. Mn(III) Center Availability as a Rate Controlling Factor in the Oxidation of Phenol and Sulfide on δ-MnO2. Environ Sci Technol. 2001; 35(16):3338–3343. [PubMed: 11529574]
69. Herszage J, dos Santos Afonso M. Mechanism of Hydrogen Sulfide Oxidation by Manganese(IV) Oxide in Aqueous Solutions. Langmuir. 2003; 19(23):9684–9692.
70. Kostka JE, Luther GWI, Nealson KH. Chemical and biological reduction of Mn(III)-pyrophosphate complexes: Potential importance of dissolved Mn(III) as an environmental oxidant. Geochim Cosmochim Acta. 1995; 59(5):885–894.
71. Oldham VE, Owings SM, Jones MR, Tebo BM, Luther GW III. Evidence for the presence of strong Mn(III)-binding ligands in the water column of the Chesapeake Bay. Mar Chem. 2015; 171:58–66.

72. Yao W, Millero FJ. The rate of sulfide oxidation by δMnO2 in seawater. Geochim Cosmochim Acta. 1993; 57(14):3359–3365.

73. Hem JD, Lind CJ. Nonequilibrium models for predicting forms of precipitated manganese oxides. Geochim Cosmochim Acta. 1983; 47(11):2037–2046.

74. Robie RA, Huebner JS, Hemingway BS. Heat capacities and thermodynamic properties of braunite (Mn7SiO12) and rhodonite (MnSiO3). Am Mineral. 1995; 80:560–575.

75. Gutzmer J, Beukes NJ. Mineral paragenesis of the Kalahari managanese field, South Africa. Ore Geol Rev. 1996; 11(6):405–428.

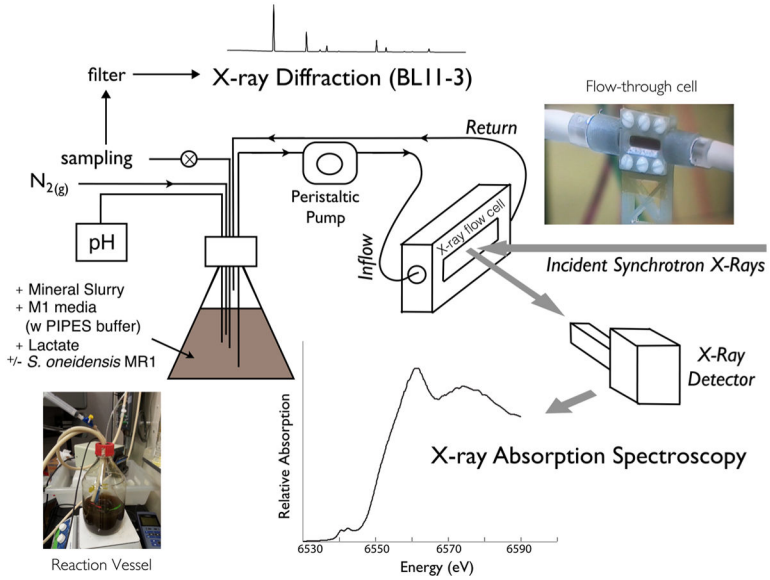

Figure 1.

Schematic of flow-through system showing reaction vessel with colloidal manganese oxide mineral slurry, M1 media with PIPES buffer, lactate, and (depending on experiment) *Shewanella oneidensis* MR-1 (MR-1). The reaction vessel was kept anoxic with N_2 and pH was measured via an environmental pH probe. A sampling portal enabled acquisition of hourly filter samples to be measured later on a synchrotron X-ray diffraction beamline. A peristaltic pump brought a representative portion of the flow-through cell through anaerobic tubing into the beamline hutch, where the X-ray beam could sample the Mn mineralogy, coordination environment, and redox state through a window on an X-ray flow through cell. The resultant X-ray absorption spectra were measured on an X-ray detector. Photos of the reaction vessel and flow-through cell are shown alongside the schematic drawing.

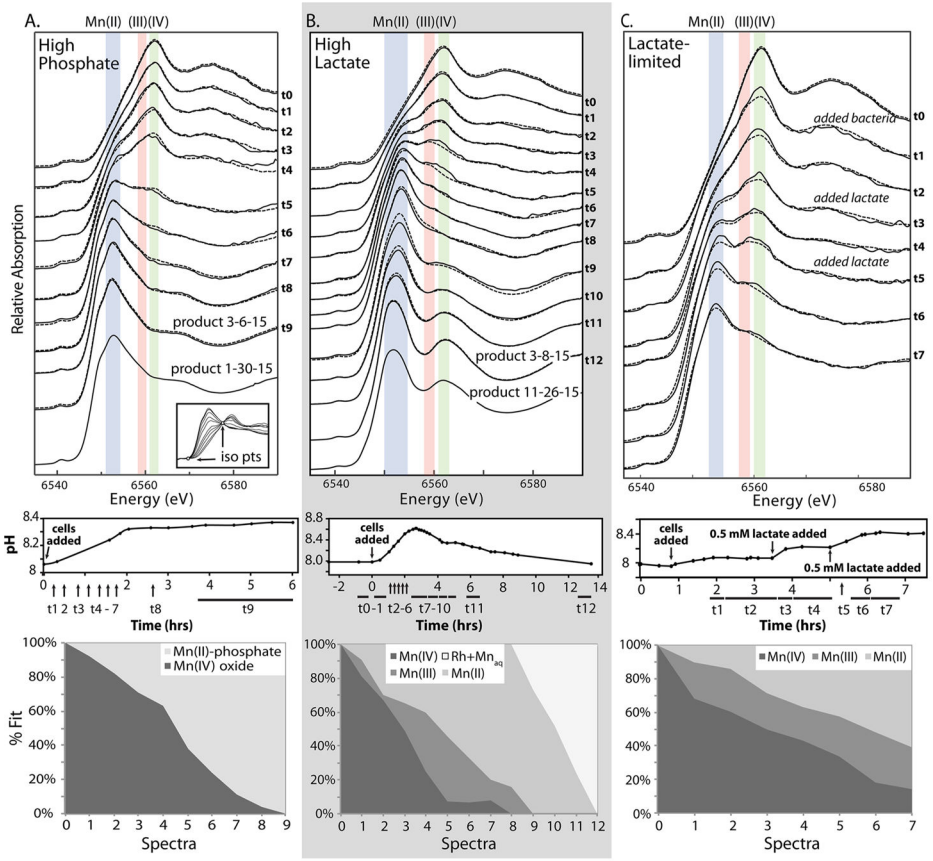

Figure 2.

Three representative microbial reduction experiments observing the reduction sequence induced by MR-1, with the initial colloidal Mn(IV)O_2 at the top and the progression of spectra (single spectra shown as arrows and averaged spectra shown as black bars in time plot below) shown descending to a final product at the bottom. Fits are shown in dashed lines overlying sample spectra. Below spectra, time course measurements of pH measurements are plotted. At the bottom, time course plots of fractional contribution of components determined by spectral fitting routines are shown. (A) High-phosphate (4.3 mM) experiment, proceeding from MnO_2 to a Mn(II)-phosphate precipitate. Isosbestic points (abbreviated “iso pts”) shown in inset. (B) High-lactate (20 mM) experiment, evolving colloidal MnO_2 to a mixture of ~75% rhodochrosite ($MnCO_3$) and ~25% aqueous Mn^{2+} ($Rh+Mn_{aq}$) through Mn^{2+} and Mn(III)OOH phases. (C) Lactate-limited experiment, beginning at 0.5 mM lactate with two further additions of 0.5 mM lactate, showing Mn(III)OOH remaining in the final spectra. See text for details and Figure S2 for comparisons between endmember spectra and standard spectra used in fits.

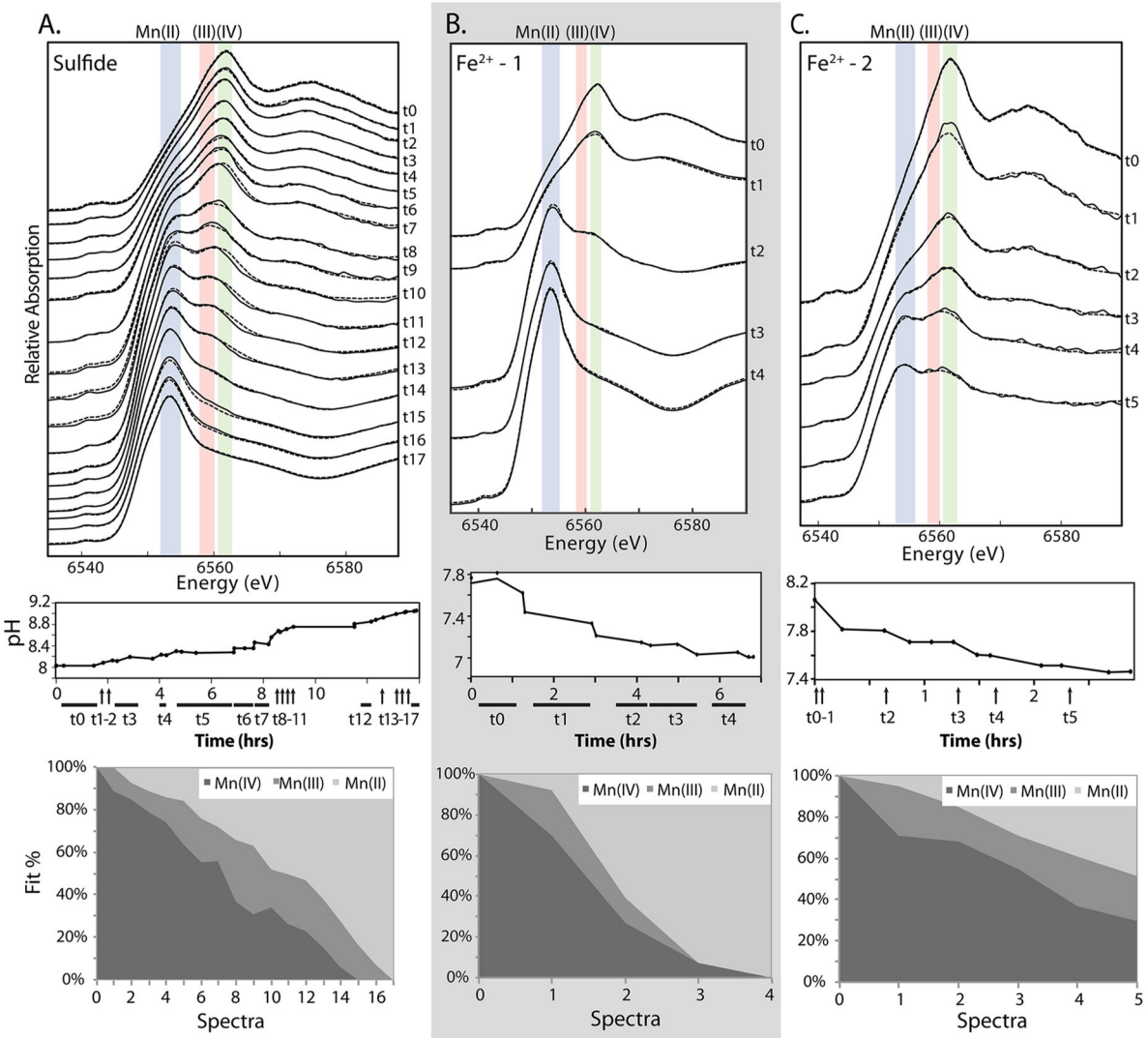

Figure 3.

Three representative abiotic reduction experiments examining the reduction sequence induced by sulfide and ferrous iron, with the initial colloidal $Mn(IV)O_2$ at the top and the progression of spectra (single spectra shown as arrows and averaged spectra shown as black bars in time plot below) shown descending to a final product at the bottom. Fits are shown in dashed lines overlying sample spectra. A time course of pH measurements is plotted below each experiment, and at the bottom of each column we show a time course plot of the fractional contribution of Mn-bearing components as chosen by fitting routines. (A) Sulfide-induced manganese oxide reduction, evolving to a Mn^{2+}-dominated solution. (B) Ferrous iron titration of manganese oxides. Mn(IV) proceeds to Mn^{2+} while pH drops with each iron addition. (C) Another representative experiment showing how ferrous iron reduces manganese. This is a limited-titrant reduction and a Mn(III) phase can be observed in the final spectra. See text for further details and Figure S2 for comparisons between endmember spectra and standard spectra used in fits.

Table 1

Overview of Experiments Performed at Stanford Synchrotron Radiation Lightsource Using Real-Time XAS Measurements to Monitor Reaction Progress

base conditions	reductant(s)	other	data shown in
Mn(IV) + *S. oneidensis*	lactate (20 mM)	+ 4.3 mM phosphate	Figure 2A, Figure S3
Mn(IV) + *S. oneidensis*	lactate (20 mM)		Figure 2B, Figures S4, S5
Mn(IV) + *S. oneidensis*	lactate (limited, 1.5 mM total)		Figure 2C
Mn(IV)	lactate (20 mM) + Na_2S		Figure 3A
Mn(IV)	lactate (20 mM) + Fe(II)		Figure 3B, Figures S6, S7
Mn(IV)	Lactate (20 mM) + limited Fe(II)		Figure 3C